Electrolyte dependence of particle motion near an electrode during ac polarization

Christopher L. Wirth,* Paul J. Sides, and Dennis C. Prieve
Department of Chemical Engineering, Carnegie Mellon University, Pittsburgh, Pennsylvania 15213, USA
(Received 18 December 2012; published 8 March 2013)

The phase angle between the imposed ac electric field and the oscillations in particle height is the key parameter governing the sign of interparticle force during two-dimensional directed assembly. The phase angle depends on a number of experimental parameters, including the frequency of the electric field and dispersing electrolytes. The origin of electrolyte dependence in this phase angle has been a mystery for a decade. Electrolyte dependence arises from polarization of the particle's diffuse layer, which affects the dynamic electrophoretic mobility of the particle. A full description of the magnitude and phase angle of the dynamic electrophoretic mobility was incorporated into a nonlinear integro-differential equation of motion for a 5.7 μm diameter particle suspended in 0.15 mM KOH, KCl, $NaHCO_3$, NH_4OH, and NaOH at frequencies between 5 and 1000 Hz. Integration of the equation revealed that the phase angles for a particle in KOH, NH_4OH, and NaOH were smaller than the phase angles calculated for a particle in KCl and $NaHCO_3$, which is consistent with previously published experiments. Although the phase angles for each electrolyte are spread over only $\sim 1^\circ$, the results cluster around 90°, which is the crucial boundary between particle aggregation ($>90^\circ$) and separation ($<90^\circ$). A family of curves of the oscillation in particle height collapsed to a master curve when the amplitude of motion was scaled with the product of the dynamic electrophoretic mobility and electric field strength. These results constitute the first *a priori* prediction of electrolyte-dependent motion of a particle near an electrode during ac polarization.

DOI: 10.1103/PhysRevE.87.032302 PACS number(s): 82.45.−h, 47.57.jd

I. INTRODUCTION

The directed motion of colloidal particles has potential applications in the preparation of photonic materials [1], the separation of colloidal dispersions and emulsions [2,3], and the high throughput evaluation of electrocatalysts [4,5]. Many investigators therefore have focused on mechanisms underlying the synthesis of two-dimensional colloidal crystals on a planar electrode [6–25]. Aggregation and separation of particles occurs in both dc and ac electric fields [6–9,11,12,15, 18,20–22,24,25]. The process is reversible and controllable because the steady structure of the assembly depends on the strength, direction, and frequency of the electric field [20,21]. Surprisingly, the steady structure also depends on the dispersing electrolyte [22]. An ensemble of particles dispersed in KCl or $NaHCO_3$ assembled into a close-packed hexagonal array upon application of a 100-Hz ac electric field, but the particles of an ensemble dispersed in NH_4OH or KOH adopted equally spaced separations of several radii despite the equivalence of all other experimental parameters [22].

Two mechanisms have been proposed to explain the aggregation and separation of two-dimensional (2D) ensembles in these circumstances. Induced charge electroosmosis (ICEO) relies on the interaction between oscillating electric field components and charge that accumulates on the electrode during polarization [15,19]. The product of the sinusoidal oscillations of electric field and charge produces a steady entraining flow and an unsteady flow at twice the frequency. Questions regarding the applicability of this model are unresolved. First, the degree of voltage polarization across the diffuse layer necessary to account for the particle motion is unlikely to be achieved. Second, the ICEO force is always attractive, which contradicts findings described in the previous paragraph. Third, distinct motion at twice the imposed frequency has never been found in real-time observations of particle motion with total internal reflection microscopy (TIRM).

The other mechanism, due to Prieve and co-workers [10,13,14,16–18], relies on a break in the antisymmetry of particle motion normal to the electrode during the two halves of each cycle. The break arises from the dependence of the entrainment velocity on the distance between the particle and the electrode. Fagan *et al.* [10,14], measuring the response of a single particle to an ac electric field in the direction normal (z axis, Fig. 1) to an electrode with TIRM, discovered a phase angle between oscillations in particle height and the electric field. A drift velocity model incorporating the phase angle [17] predicted that an isolated pair of particles separated when the phase angle was $<90^\circ$, but the same isolated pair aggregated when the phase angle was $>90^\circ$. Hoggard *et al.* [18] systematically measured the interparticle distance of an isolated pair of particles suspended in a variety of electrolytes. Predictions from the drift velocity model, which incorporated the experimentally measured phase angles, were in good quantitative agreement with experimental measurements of the net motion of isolated particles. The discovery of Fagan *et al.* [10,14] that a phase angle differing from 90° is required for net motion of particle pairs, and the confirming experiments of Hoggard *et al.* [18] provided strong evidence that a combination of short-range electrophoresis and electroosmosis, with modifications due to the proximity of the particles to the electrode, drives 2D directed assembly in ac electric fields.

Wirth *et al.* [24] developed a model that demonstrated the possibility of phase angles less than or greater than 90°. Newton's second law, including dynamic friction, linearized colloidal forces, particle and fluid inertia, and the

*Current address: Department of Chemical Engineering, Katholieke Universiteit Leuven, B-3001 Leuven, Belgium; email address: chris.wirth@cit.kuleuven.be

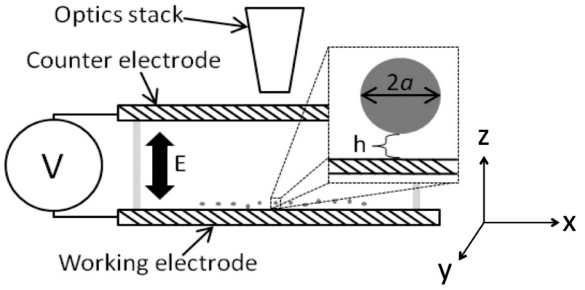

FIG. 1. Illustration of the experimental setup. An ac potential is applied across a parallel plate electrochemical cell filled with electrolytes. Particles have a radius a and are separated a distance, h, from the working electrode. The parallel plate electrodes, each with an area of 10.24 cm^2, were separated by 1.4 mm in the experiments simulated here. An optics stack comprising an optical microscope, a CCD camera, and a photomultiplier tube is positioned above the fluid cell. More details on the experimental setup can be found in Ref. [18].

electrophoretic force arising from an ac electric field, was the basis of the model. The analytical solution to this problem predicted a phase angle that could be either $<90^\circ$ or $>90^\circ$, depending on the frequency. The model resembled those found in the dynamic electrophoresis literature, except for the addition of a colloidal force field. The model demonstrated a physical origin of the phase angle and its frequency dependence.

The present contribution refines this model [24] to more realistic representations of the forces, including physicochemical differences between electrolytes. We numerically solved the nonlinear integro-differential equation of motion for a particle near an electrode during ac polarization. The model comprises an expolinear colloidal potential energy well, a wall-enhanced dynamic drag, and dynamic electrokinetic forces. Electrolyte dependence enters the problem through a full description of the dynamic electrophoretic mobility of the particle and through the conductivity of the dispersing electrolyte for a given ionic strength. The phase angle, the crucial parameter determining the direction of assembly, was calculated as a function of frequency for a single particle dispersed in KOH, KCl, $NaHCO_3$, NH_4OH, and NaOH under conditions identical to those used in previous experiments [18].[1] The phase angle depended on the dispersing electrolyte. The phase angles cluster around 90°, the boundary that determines whether particles aggregate or separate. This is the first demonstration of the mechanism by which the choice of electrolyte affects directed assembly. Moreover, the results show how a subtle effect can produce binary results; a slight change of phase angle causes particles to aggregate or separate.

[1]Experiments in Ref. [18] also included H_2CO_3 as one of the dispersing electrolytes. Based on the pH reported by the authors, we calculated an H_2CO_3 concentration to be 0.0025 mM, which was far smaller than the concentration of all other electrolytes used in Ref. [18] (see Table II). An electrolyte concentration of 0.0025 mM would correspond to a Debye length of 192 nm and an equilibrium particle height of nearly 2 μm, which is outside the range of observation with a TIRM; we decided not to include H_2CO_3 in the work presented here because of this inconsistency.

II. THEORY

Consider a particle of radius a and mass M_p separated from an electrode by a distance h (see Fig. 1). An ac electric field normal to the electrode drives the oscillatory motion of the particle along the z axis. The equation of motion of the particle is

$$M_p \frac{d^2h}{dt^2} = F_c + F_d + F_e, \tag{1}$$

where F_c is the summation of colloidal forces, F_d is the dynamic drag, and F_e is the sum of the electrophoretic force F_{ep} and the dielectrophoretic force F_{dep}, which arise from interaction of the particle with the applied electric field.

A. Colloidal forces

The particle samples a potential energy well (Φ_c) comprising electrostatic repulsion arising from overlap of the diffuse counterion clouds on the particle and electrode surfaces, van der Waals interactions, and gravity. Typically, the particles and electrode material have a bound negative charge; like charges on the two surfaces prevent deposition and immobilization. The potential energy well has an "expolinear" shape resulting from the exponential decay of electrostatic repulsion and van der Waals attraction with height and the linear increase of gravitational potential with height. The colloidal force F_c equals the negative gradient of the potential energy:

$$F_c(h) = -\frac{d\Phi_c}{dh} = \kappa B \exp(-\kappa h) - 6.8\lambda kT \exp(-\lambda h) - G, \tag{2}$$

$$B = 64\pi\varepsilon_0\varepsilon_f a \left(\frac{kT}{e}\right)^2 \tanh\left(\frac{e\zeta_p}{4kT}\right)\tanh\left(\frac{e\zeta_e}{4kT}\right), \tag{3}$$

$$\kappa = \sqrt{\frac{2e^2C_\infty}{\varepsilon_0\varepsilon_f kT}}, \tag{4}$$

$$G = \frac{4}{3}\pi a^3(\rho_p - \rho_f)g, \tag{5}$$

where ε_f is the dielectric constant of water, ε_0 is the dielectric permittivity of a vacuum, k is Boltzmann's constant, T is temperature, e is the elementary charge, C_∞ is the bulk number concentration of electrolyte, κ^{-1} is the Debye length, $\lambda^{-1} =$ 48 nm is a decay length characteristic of the van der Waals attraction, ζ_p and ζ_e are the particle's and electrode's Stern potential. The first term in Eq. (2) represents double-layer repulsion under conditions of weak overlap of the electric double layers ($\kappa h \gg 1$). The Debye parameter defined by Eq. (4) is for 1-1 electrolytes. The second term in Eq. (2) is an empirical fit to van der Waals attraction directly measured under very similar conditions and for $h > 50$ nm [13]. Under these conditions, van der Waals attraction is severely retarded and screened [13].

B. Dynamic drag force

The dynamic drag F_d on the particle is the sum of the wall corrected Stokes drag, the added inertia, and the Basset

force:

$$F_d = -\left(\frac{f_\infty}{q(h)}\frac{dh}{dt} + \frac{1}{2}M_f\frac{d^2h}{dt^2} + 6\eta a^2\sqrt{\frac{\pi\rho_f}{\eta}}\int_{-\infty}^{t}\frac{d^2h(t')}{dt'^2}\frac{dt'}{\sqrt{t-t'}}\right), \quad (6)$$

$$q(h) = \frac{6h^2+2ah}{6h^2+9ah+2a^2}. \quad (7)$$

Here f_∞ is the linear quasisteady Stokes drag coefficient ($f_\infty = 6\pi\eta a$), $q(h)$ is the wall correction factor [26], and M_f is the mass of the fluid displaced by the particle. Although quasisteady Stokes drag is familiar, the remaining two terms in F_d might be unfamiliar. The second term on the right-hand side of Eq. (6) is the "added inertia" required to move fluid from the path of the oscillating particle. The third term is the Basset or "history" force, which accounts for the transient development of the momentum boundary layer enveloping the particle. The final two terms in Eq. (6) are obtained by solving the Navier-Stokes equation on an oscillating particle in an infinite fluid domain, retaining the linear momentum accumulation term (dv/dt), but neglecting the nonlinear inertial term ($\boldsymbol{v}\cdot\nabla\boldsymbol{v}$), where $\boldsymbol{v}$ is the velocity of the particle. Relative to viscous forces, the nonlinear inertial term is on the order of the Reynolds number ($va\rho_f/\eta$), which is small. Relative to viscous forces, the linear inertial term is on the order of the product of the Reynolds and Strouhal numbers ($N_{RS} \equiv a^2\omega\rho_f/\eta$), which is not necessarily small.

The authors are unaware of any wall correction for the final two terms in Eq. (6). However, a correction is likely unnecessary because the time for diffusion of momentum across the gap is much shorter than the period of oscillation of the particle. Then the lubrication approximation (used to predict the greatly enhanced viscous drag when $h \ll a$) will be quasisteady. More details about dynamic drag can be found in Kim and Karrila [27].

For use in the next section, consider purely sinusoidal oscillations in the particle's velocity; complex exponentials represent their time dependence. After replacing dh/dt by $\tilde{U} = U_0 e^{-i\omega t}$ and F_d by $\tilde{F}_d = F_{d0}e^{-i\omega t}$, Eq. (6) becomes $\tilde{F}_d = -\tilde{f}\tilde{U}$, where the complex drag coefficient is given by [27]

$$\tilde{f} = \left[\frac{1}{q(h)} + (1-i)\sqrt{\frac{\rho\omega a^2}{2\eta}}\right]6\pi\eta a - \frac{i\omega M_f}{2}. \quad (8)$$

Note that $q(h) = 1$ in Kim and Karrila [27]. When q depends on h, Eq. (6) becomes nonlinear in h, which would distort the response $\tilde{U}$ from a pure sinusoid or a single complex exponential. To obtain the approximation above, we assumed that the amplitude of oscillations in h are small enough that $q(h)$ can be replaced by its average value over one cycle.

C. Electrophoretic force

We define the electrophoretic force F_{ep} to be equal in magnitude but opposite in direction to that force $F_{ext}(= -F_{ep})$, which must be applied externally to a charged sphere to suppress any electrophoresis caused by a macroscopically uniform electric field, E. The linearity of Stokes equations makes the electrophoretic flow caused by the action of the electric field on the charged particle superimposable on the Stokes flow caused by the action of the external force. If the force F_{ext} were not applied, the particle would undergo electrophoresis at speed $U = \mu E$, where μ is the electrophoretic mobility of the particle. To suppress this movement, we apply F_{ext}, which (in the absence of the electric field) causes steady movement of the particle at speed $-U = F_{ext}/f$, where f is the friction coefficient for motion of the particle through an otherwise stagnant fluid. Eliminating U and F_{ext} leads to the prediction that

$$F_{ep} = QE, \quad (9)$$

$$Q = \mu f, \quad (10)$$

where Q is defined as the proportionality constant between E and F_{ep}. Although it has units of coulombs and we call it the "apparent electrokinetic charge," Q does not represent the true charge affixed to the particle. For $\kappa a \gg 1$, the ratio of Q to the true charge is $O[(\kappa a)^{-1}]$ owing to nearly complete neutralization of the true charge by the surrounding counterion cloud [24].

The above description for a steady electric field can be adapted to an oscillating field. If the electrophoretic velocity and the electrophoretic force are represented by complex exponentials ($\tilde{E} = E_0 e^{-i\omega t}$, $\tilde{U} = U_0 e^{-i\omega t} = \tilde{\mu}\tilde{E}$, and $\tilde{F}_{ep} = F_{ep0}e^{-i\omega t}$), then the electrophoretic mobility and drag coefficient also become complex quantities ($\tilde{\mu}$ and $\tilde{f}$), where their real and imaginary parts represent the in-phase and out-of-phase components of the response. When the particle is far from the electrode, we can eliminate colloidal and dielectrophoretic forces from Eq. (1), leaving $F_e = \tilde{F}_{ep}$ and $F_d = \tilde{F}_d = -\tilde{f}\tilde{U}$. Then Eq. (1) yields $\tilde{F}_{ep} = (\tilde{f} - i\omega M_p)\tilde{U}$. Substituting $\tilde{U} = \tilde{\mu}\tilde{E}$ yields

$$\tilde{F}_{ep} = \tilde{Q}\tilde{E}, \quad (11)$$

$$\tilde{Q} = (\tilde{f} - i\omega M_p)\tilde{\mu}. \quad (12)$$

Substituting $\tilde{f}$ from Eq. (8) yields

$$\tilde{Q} = \left\{\left[\frac{1}{q(h)} + \left(1-i\right)\sqrt{\frac{\rho\omega a^2}{2\eta}}\right]6\pi\eta a - i\omega M\right\}\tilde{\mu}, \quad (13)$$

where $M = M_p + (1/2)M_f$ is the total inertial mass of the fluid and particle. Note that in the limit of $\omega \to 0$, Eq. (13) reduces to Eq. (10).

When colloidal forces, dielectrophoresis, and the height dependence of various coefficients are considered, Eq. (1) becomes nonlinear in the dependent variable $h(t)$. Then purely sinusoidal oscillations in $E(t)$ produce nonsinusoidal oscillations in $h(t)$. In numerical solutions of Eq. (1) we abandon the use of complex exponentials and solve the equation using purely real quantities. In particular, we need the real part of the electrophoretic force given by Eqs. (11) and (13). If the electric field is represented as $E(t) = E_0\cos(\omega t)$,

then the electrophoretic force is

$$F_{ep} = \left[\left(\frac{1}{q(h)} + \sqrt{\frac{N_{RS}}{2}}\right) f_\infty \cos(\omega t + \phi) - \left(\omega M + f_\infty \sqrt{\frac{N_{RS}}{2}}\right) \sin(\omega t + \phi)\right] \mu_0 E_0, \quad (14)$$

where μ_0 and ϕ are the absolute magnitude and phase angle of the complex dynamic electrophoretic mobility $\tilde{\mu} = \mu_0 e^{-i\phi}$ (DEM) of a particle in an infinite sea of fluid. Here, the phase angle and magnitude of the DEM were calculated with a commercially available code [28–32]. Although the code was tailored for ensembles of particles, a sufficiently small volume fraction (10^{-6}) ensured that particle-particle effects were negligible.

D. Dielectrophoretic force

Dielectrophoretic force arises from the polarization of the charge at the particle and the subsequent interaction between the electric field and the effective dipole. The net dielectrophoretic force on a particle in a uniform field far from a boundary vanishes but is nonzero when the particle is close to a boundary, another dipole, or in an externally controlled electric field gradient. Dietz [33] provides the following approximation for the dielectrophoretic force when a dielectric particle is immersed in a conductive liquid near a planar interface:

$$F_{dep} = D\tilde{E}^2, \quad (15)$$

$$D(h) = -\frac{3\pi\varepsilon_0\varepsilon_f a^2}{1 + e^{-4\delta}} (1+\delta)^{-4} \left(\frac{1}{8}\right), \quad (16)$$

where $\delta = h/a$. The real part of the electric field in Eq. (15) was taken to obtain $\mathrm{Re}(\tilde{E}) = E_0 \cos(\omega t)$. Squaring this result produced a steady and oscillating term with a frequency of 2ω; both terms were included in the numerical integration scheme.

III. NUMERICAL ALGORITHM

Equation (1) is a nonlinear integro-differential equation. The Basset integral required temporal integration of all past positions of the particle. A successive approximation technique was used to overcome this problem. The algorithm was initiated by numerically integrating Eq. (1) without the Basset integral and with the following initial conditions:

$$h(0) = \frac{1}{\kappa} \ln\left(\frac{\kappa B}{G}\right), \quad (17)$$

$$h'(0) = 0, \quad (18)$$

where Eq. (17) is the most probable height of the particle in the absence of an applied electric field. The result of the initial iteration was a slow transient leading eventually to stationary oscillations in particle height. Once stationary oscillations in particle height were achieved, the final period of oscillations in height were fitted with a Fourier series, which captured any nonlinearity in the stationary oscillations of height. The next iteration was then calculated with the Basset force term evaluated using a Fourier series representation (see next paragraph) and initial conditions matching those of the final point calculated in the previous iteration. An adaptive numerical integrator capable of calling on an Adams-Bashforth method for nonstiff systems or a backward differential method for stiff systems was used for the numerical integration conducted for each iteration. Many cycles (between 25 and 1000), each of which contained 100 time steps, were computed for each iteration to ensure that the particle reached steady oscillations in height. The number of cycles required to reach steady oscillations depended on the frequency of the electric field. Lower frequencies required fewer cycles to be simulated. Table I summarizes the global variables used in the simulations. Figure 2 shows an example of convergence during the successive approximation algorithm.

TABLE I. Global parameters used for all calculations.

Water viscosity, η (Pa s)	0.000 890 416
Particle radius, a (m)	0.000 002 85
Elemental charge, e (C)	1.602 18E-19
Boltzmann's Constant, k (J/K)	1.380 65E-23
Avogadro's number, N_A (#/mol)	6.022 14E + 23
Molar gas constant, R (J/mol K)	8.314 47
Dielectric permittivity of a vacuum, ε_0 (F/m)	8.854 19E-12
Dielectric constant of water, ε_f	78.36
Dielectric constant of the particle, ε_p	2.6
Temperature, T (K)	298
Faraday's constant, F (C/mol)	96 485.339
Density of fluid, ρ_f (kg/m^3)	1000
Density of the particle, ρ_p (kg/m^3)	1055
Electrode ζ potential, ζ_e (mV) (KOH, NaOH, $NaHCO_3$, NH_4OH)	−80
Electrode ζ potential, ζ_e (mV) (KCl)	−30

The Basset integral appearing in Eq. (1) required integration of all prior particle positions, which slowed the convergence and is complicated by the nonsinusoidal oscillations in height

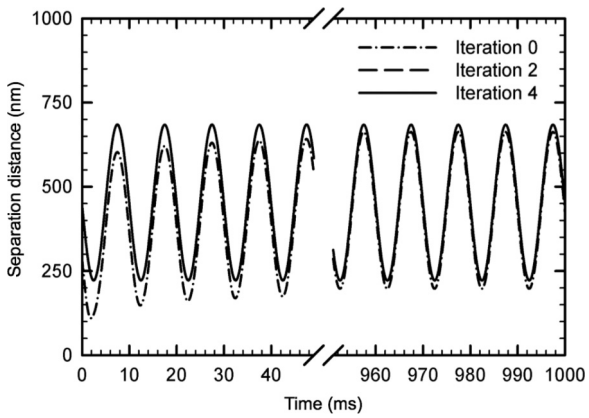

FIG. 2. Illustration of convergence of the successive approximation algorithm for a particle suspended in 0.15 mM KOH and exposed to an electric field of 100 Hz and 1778 V m^{-1}. One hundred cycles and 100 time steps per cycle were calculated for each iteration. A total of four iterations were conducted, with the initial (iteration 0), second (iteration 2), and fourth (iteration 4) shown here. Iterations 2 and 4 are indistinguishable from each other because the calculation has converged by the second iteration.

experienced by the particle. We avoided these difficulties by using a Fourier series (FS) to represent the steady oscillations in height from the previous iteration accurately and then computing the Basset integral without the integration step. The FS approximation $H(t)$ of an arbitrary periodic function $x(t)$ having period $2\pi/\omega$ is as follows:

$$a_0 = \frac{\omega}{2\pi}\int_{-\pi/\omega}^{\pi/\omega} x\,(t)\,dt, \tag{19}$$

$$a_n = \frac{\omega}{\pi}\int_{-\pi/\omega}^{\pi/\omega} x\,(t)\cos\,(n\omega t)\,dt, \tag{20}$$

$$b_n = \frac{\omega}{\pi}\int_{-\pi/\omega}^{\pi/\omega} x\,(t)\sin\,(n\omega t)\,dt, \tag{21}$$

$$H\,(t) = a_0 + \sum_{n=1}^{N}\left[a_n\cos\,(n\omega t) + b_n\sin\,(n\omega t)\right], \tag{22}$$

where a_0, a_n, and b_n are the FS coefficients and N is the number of terms in the truncated FS. Inserting Eq. (22) into the Basset force integral and simplifying gives

$$6\eta a^2\sqrt{\frac{\pi\rho_f}{\eta}}\int_{-\infty}^{t}\frac{d^2H}{d\tau^2}\frac{d\tau}{\sqrt{t-\tau}} = -f_\infty\sqrt{\frac{a^2\rho_f}{2\eta}}\sum_{n=1}^{N}(n\omega)^{3/2}\left[(a_n - b_n)\cos\,(n\omega t) + (a_n + b_n)\sin\,(n\omega t)\right]. \tag{23}$$

Equation (23) avoided the numerical integration of all past positions of the particle. The FS expression for the Basset force term only required a single cycle of the particle's steady oscillations in height to compute the FS coefficients given from Eqs. (19) to (21).

Oscillations in particle height became nonsinusoidal at sufficiently low frequency or large electric field strength, which caused deviations from sinusoidal behavior. Three FS terms were sufficient to accurately approximate these steady oscillations in particle height for all conditions. The error between the calculated oscillations in particle height and the FS fit was computed by subtracting those two quantities and scaling the difference by the amplitude of oscillation. The largest error in the FS fit was 1.00%. In addition, the FS fit was used to find the location of minimum in oscillations, which was required to determine the phase angle between the oscillations in height and the electric field. This definition of the phase angle was consistent with the definition used previously [18]. Figure 3 shows the "worst case scenario" fit and the location of the minimum in height.

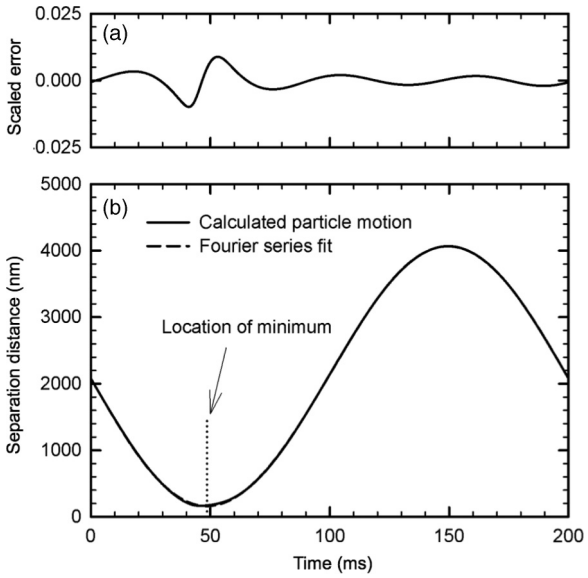

FIG. 3. Worst case scenario for the Fourier series (FS) fit of oscillations in particle height. (a) Scaled percent error of fit shown in panel (b). The error between the calculated oscillations in particle height and the FS fit was computed by subtracting those two quantities and scaling the difference by the amplitude of oscillation. The maximum error was 1.00%. (b) Comparison between the FS fit and the motion of the particle. The largest error occurred at the bottom of the cycle where nonlinear colloidal forces are important. The conditions of this calculation were an electric field frequency of 5 Hz and a strength of 848 V/m at an electrolyte concentration of 0.15 mM NH_4OH.

IV. RESULTS

A. The dynamic electrophoretic mobility $\tilde{\mu}$

The magnitude and phase angle of the DEM was a required input for the definition of $\tilde{Q}$ used in the numerical integration of Eq. (1). The DEM of a particle suspended in KOH, KCl, $NaHCO_3$, NH_4OH, and NaOH electrolyte solution was calculated as a function of frequency under conditions chosen to match those of published experimental work [18]. Hoggard *et al.* [18] used dynamic light scattering to measure the static electrophoretic mobility of an ensemble of particles and the ζ potential was calculated with Henry's equation. Here, we recalculated the ζ potential of the ensemble of particles dispersed in each electrolyte using the algorithm of O'Brien and White [34]. Table II summarizes these data.

Figure 4 shows results for the scaled magnitude and phase angle of the DEM of a particle in each electrolyte. The magnitude of the DEM was scaled by the static electrophoretic mobility shown in Table II. As expected, the scaled DEM approached unity as frequency $\rightarrow$ 0 Hz. The magnitude of the DEM increased slightly as frequency was increased for all electrolytes. At higher frequencies that are not shown, the magnitude of the DEM decreased because of the increased importance of particle inertia. A similar effect was observed on the phase angle of the DEM. The phase angle approached 0° at very low frequencies for all electrolytes. As frequency increased, the phase angle for all electrolytes increased above 0° and reached a maximum.

B. Linear problem

The numerical algorithm presented in Sec. III was tested by solving a linearized version of Eq. (1) published elsewhere [24]. The linearized model assumed that the particle was far from the wall, the solution had a thin Debye length ($\kappa a \rightarrow \infty$), and the particle was restricted to a parabolic potential energy well: $\phi\,(h) = (1/2)\kappa G(h - h_m)^2$. Equation (13) was used for the apparent electrokinetic charge, but with $q = 1$. Figure 5 summarizes results from this test.

TABLE II. Electrolyte data.

Electrolyte	Concentration (mM)	Conductivity (μS/cm)	κa	pH	ζ potential[a] (mV)	$f(\kappa a)$	Electrophoretic mobility [μm cm/(V s)]	ζ potential[b] (mV)
KOH	0.1500	40.72	114.78	9.8	−105	1.463	−7.982	−120
KCl	0.1500	22.47	114.78	5.8	−78	1.463	−5.930	−82
$NaHCO_3$	0.1500	14.19	114.78	9.4	−96	1.463	−7.298	−108
NH_4OH	0.1500	40.73	114.78	9.2	−95	1.463	−7.222	−104
NaOH	0.1500	37.21	114.78	9.7	−104	1.463	−7.906	−122

[a]Zeta potential of particles reported by Hoggard *et al.* [18].
[b]Zeta potential of particles recalculated with the algorithm of O'Brien and White [34].

At low frequency, the phase angle between the position of the particle and the electric field approached 0°. This phase angle is crucial to the drift velocity model; henceforth this parameter shall just be called the "phase angle." The low-frequency behavior was a consequence of the colloidal force field that balanced the electrophoretic force in this frequency regime. The particle can be considered to be at its equilibrium height at every instant in the limit of frequency → 0 Hz. The phase angle approached 90° as frequency increased because viscous damping (i.e., Stokes drag) balanced the electrophoretic force at low frequency. At high frequency, the phase angle responded to an increase in the importance of inertia. Figure 5(b) shows the "apparent DEM," which is not equal to the actual DEM of the particle. The apparent DEM is equal to the quotient of the maximum velocity and the electric field. The apparent DEM was heavily damped at low frequency by the colloidal potential energy well, increased towards the force-free mobility limit of Helmholtz-Smoluchowski at intermediate frequencies, and then decreased slightly above 1 kHz because of the increased importance of inertia of the

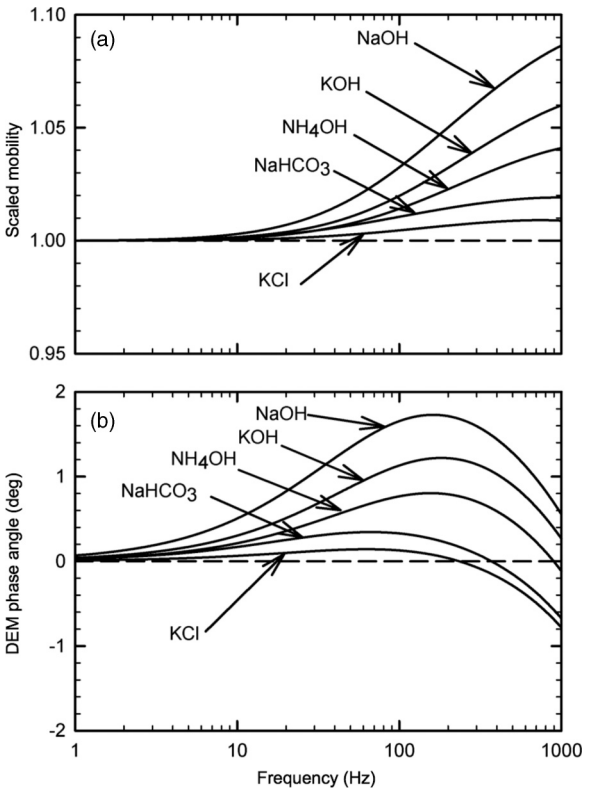

FIG. 4. Computed dynamic electrophoretic mobility (DEM) of a particle in a variety of electrolytes. (a) The magnitude of the DEM scaled by its low-frequency value. (b) The phase angle of the DEM. Both the magnitude and the phase angle of the DEM were electrolyte dependent.

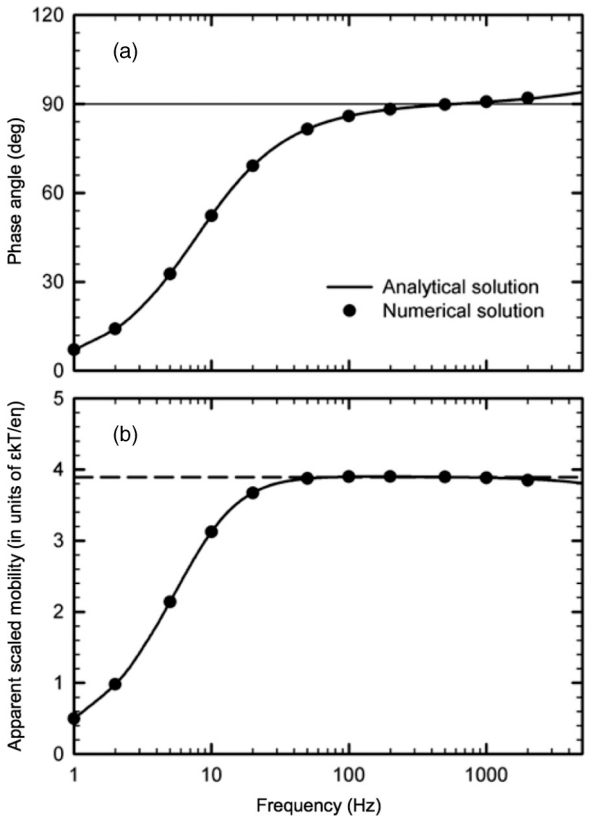

FIG. 5. Test of numerical integration algorithm described in Sec. III. (a) Particle position phase angle and (b) the "apparent scaled mobility" as a function of frequency for the analytical and numerical solutions. Strong quantitative agreement was found between the two solutions for both quantities. The data plotted in (b) is called the "apparent scaled mobility" because it is the velocity divided by the electric field strength, not the actual dynamic electrophoretic mobility. The apparent scaled mobility decreased as frequency decreased because the colloidal force field damped the motion of the particle. The broken line in (b) is the mobility limit given by Helmholtz-Smoluchowski for $\kappa a \to \infty$.

fluid-particle system. These results demonstrated the validity of the numerical integration algorithm.

C. Nonlinear problem

Equation (1) was integrated with the numerical algorithm described in Sec. III and tested in Sec. IV B. The primary differences between the problem solved here and the linear test problem were that the nonlinear problem includes (1) hydrodynamic effects resulting from the proximate boundary [i.e., $q(h)$ different from unity]; (2) an expolinear potential energy well (instead of a parabolic harmonic potential well) comprising more realistic electrostatic interactions, gravity, and van der Waals interactions; (3) an expression that accounted for the dielectrophoretic attraction between the particle and boundary; and (4) electrophoretic forcing that included a full description of the apparent electrokinetic charge, as described by Eq. (14).

The calculations were carried out for a 5.7 μm-diameter particle suspended in KOH, KCl, $NaHCO_3$, NH_4OH, or NaOH at a variety of electric field frequencies. An ac voltage of 5 V peak-to-peak (2.5 V amplitude) was "applied" between parallel plate electrodes, each with an area of 10.24 cm^2 and separated by 1.4 mm. The nominal electric field strength is given by the quotient of the peak voltage and the electrode separation. However, the electric field strength in solution, which acts on the particle, is the quotient of the current density and the electrolyte conductivity. The current density as a function of frequency was calculated from the impedance of a resistor and a capacitor in series. A model incorporating a resistor (R) and capacitor (C) in series is often called an RC circuit model. The resistance of the bulk electrolyte solution was calculated by dividing the cell constant by the electrolyte conductivity, where the cell constant is the distance between the working electrode and the reference electrode divided by the area of the electrode. The capacitance of the electric double layer of the electrode was measured in an earlier work to be approximately 10 $\mu F/cm^2$ [24]. Solution and particle properties are summarized in Table II.

Figure 6 summarizes results from the solution of Eq. (1). Figure 6(a) shows that the electric field inversely depends on the electrolyte conductivity at constant ionic strength and frequencies below 50 Hz for which the impedance associated with double-layer polarization is not negligible compared to the ohmic resistance of the electrically neutral bulk solution. Based on an RC circuit model, the reduction in the electric field strength from its limiting value of 2.5 V divided by 1.4 mm (1786 V/m) depends solely on the frequency relative to the characteristic frequency $(RC)^{-1}$ for which in-phase and out-of-phase components of the current are equal. Electrolytes having higher conductivities also have higher characteristic frequencies, which shifts the curves to the right as conductivity increases. (The ionic strength was held constant in order to make the Debye length consistent from electrolyte to electrolyte in the calculations and experiments, but this introduced an effect of electric field at low frequency.) At frequencies above 50 Hz, the electric field approached the limiting value for all electrolytes because the impedance of the double-layer capacitance in the system becomes negligible. Note that we did not report the electric field strength in Fig. 5, although it too varies with frequency. In the linear theory, all the amplitudes are linear in the electric field strength and the phase angle does not depend on it.

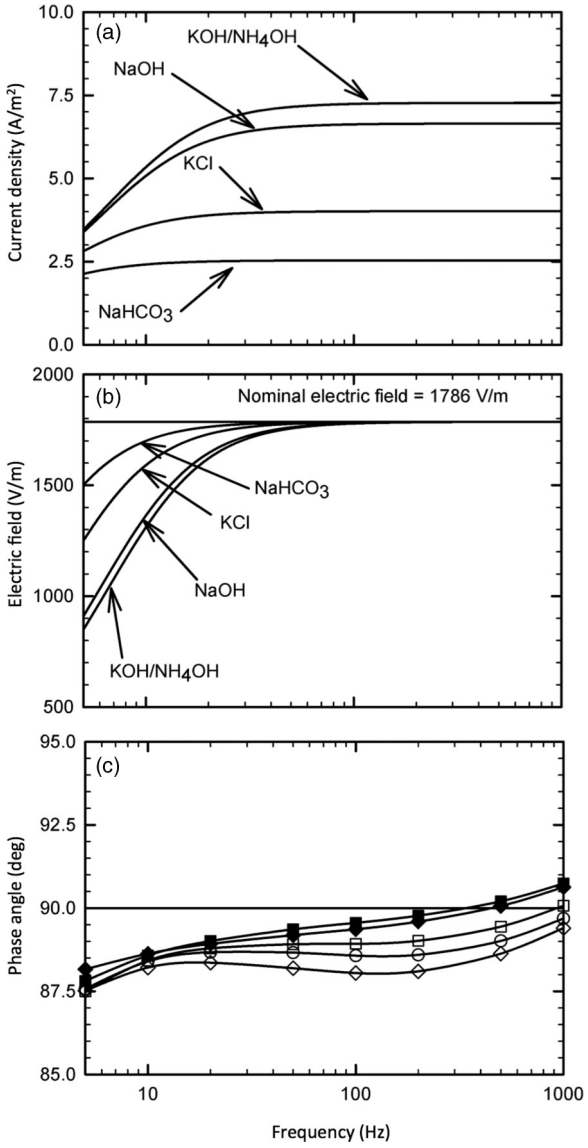

FIG. 6. Solution of Eq. (1) for a particle in a variety of electrolytes. (a) The current density and (b) the electric field strength for each electrolyte. The electric field strength depended on the electrolyte conductivity at frequencies <50 Hz. When the frequency >50 Hz, the electric field in solution reaches its nominal value, which is the quotient of the applied potential and electrode separation distance (i.e., 2.5 V/1.4 mm = 1786 V/m). (c) The particle position phase angle for KOH (open circles), KCl (solid squares), $NaHCO_3$ (solid diamonds), NH_4OH (open squares), and NaOH (open diamonds). These data show that the phase angle was electrolyte dependent.

Figure 6(c) shows that the phase angle was less than 90° at low frequency, approached 90° as frequency increased, and then crossed 90° at a sufficiently high frequency. The low-frequency behavior was a consequence of the growing importance of colloidal forces and the decrease in electric field strength. Phase angles were closer to 90° for the entire frequency regime than those reported in Fig. 5(a). The phase angles were closer to 90° because of the greater importance of

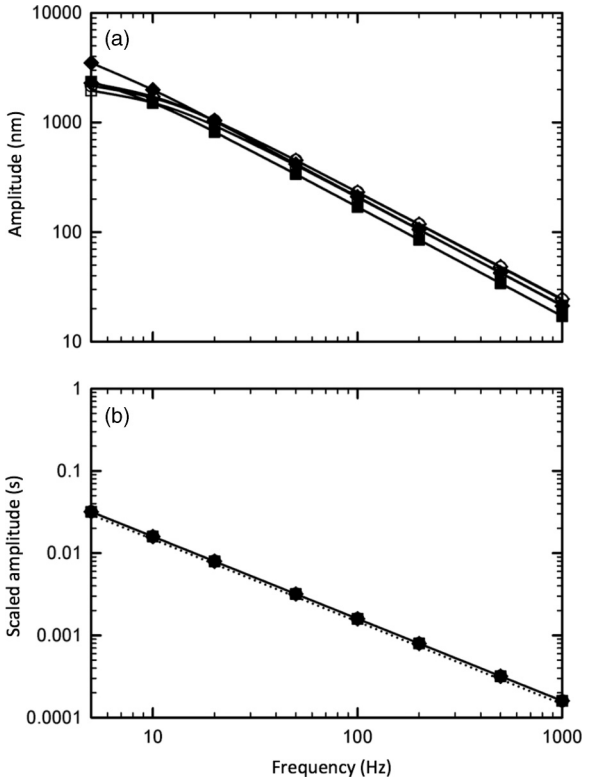

FIG. 7. Amplitude of oscillations in particle height for KOH (open circles), KCl (solid squares), $NaHCO_3$ (solid diamonds), NH_4OH (open squares), and NaOH (open diamonds). (a) The amplitude of oscillations in height were electrolyte dependent and typically between 10 and 1000 nm. (b) Scaling the amplitude of oscillations by the product of the electric field strength and dynamic electrophoretic mobility collapsed the family of curves from panel (a) onto a master curve. The dotted line in panel (b) is the linear solution described in Sec. V B. The dotted line was obtained by solving Eq. (1) with $Q = \mu_s f/q(h)$ and $q(h)$ evaluated at $h(0)$.

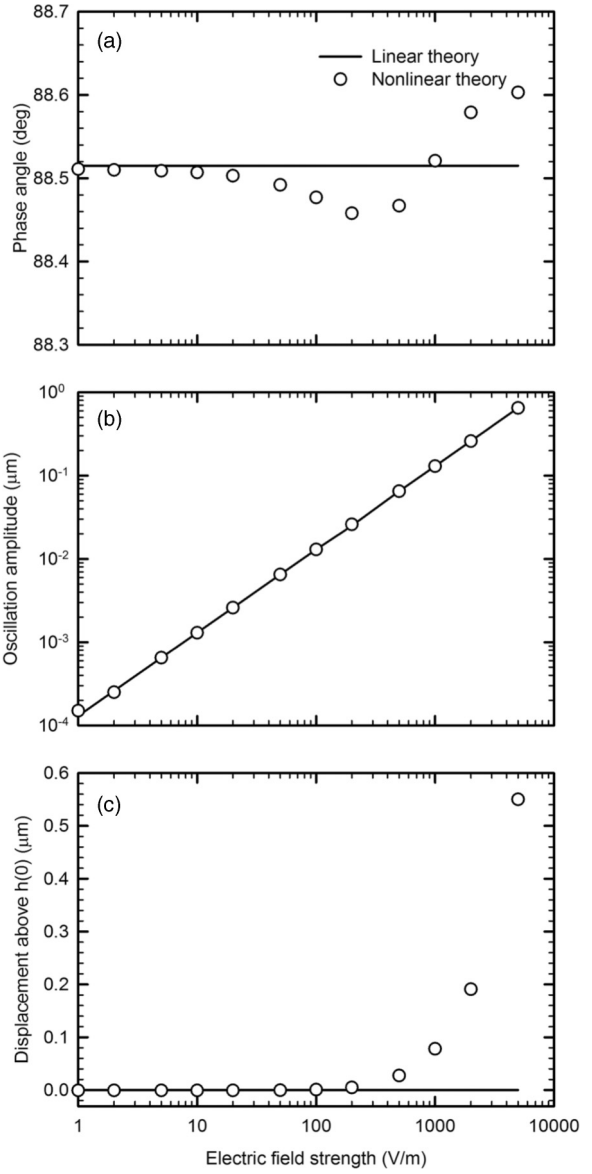

FIG. 8. Comparison of the linear and nonlinear models for a particle in 0.15 mM KOH at varying electric field strengths and a fixed frequency of 100 Hz. These two models produce similar results for (a) the phase angle and (b) the amplitude of oscillation. However, the nonlinear model predicts substantial displacement away from $h(0)$, while the linear model predicts no displacement away from $h(0)$.

the quasisteady Stokes drag when the effect of proximity to the wall is included. The Stokes drag term in Eq. (8) is multiplied by q^{-1} [26], which increases its value by approximately an order of magnitude compared to Fig. 5(a) which assumes the particle is far from the wall and $q = 1$. Also, for a broad frequency range, the phase angles were separated by a few degrees depending on the dispersing electrolyte. The phase angles calculated for a particle in KOH, NH_4OH, and NaOH tended to have phase angles smaller than those calculated for a particle in KCl and $NaHCO_3$.

Figure 7 shows the amplitude of oscillations in $h(t)$. The amplitude was calculated by subtracting the minimum from the maximum height (during the final full cycle) and dividing by 2. Just like the phase angle in Fig. 6, the amplitude was a function of frequency and the dispersing electrolyte. The differences in the amplitude stemmed from differences in the electrophoretic driving force for each electrolyte. A larger driving force produced a larger amplitude of oscillation. The magnitude of the driving force was controlled by the electric field strength and the dynamic electrophoretic mobility. Thus the amplitude was scaled with the product of these two quantities. The result, shown in Fig. 7(b), was the scaled amplitude with a dimension of time. This scaling collapsed the curves of Fig. 7(a) to a single master curve. Figure 7(b) includes a dotted line that represents the predictions of the linear model, except that the wall correction q^{-1} for the Stokes drag was included. This line was obtained by solving Eq. (1) with $Q = \mu_s f_\infty/q(h)$ and $q(h)$ evaluated at $h(0)$. The data in Fig. 7 show only a small difference between the amplitude calculated with the full nonlinear model and the amplitude calculated with the linear model over a broad frequency range.

Figure 8 compares the results obtained with the linear (including q^{-1}) and nonlinear models as a function of electric field strength for a fixed frequency of 100 Hz, which is relevant to many previously conducted experiments. Figures 8(a)–8(c) show the phase angle, amplitude, and displacement of the

center of oscillations from h(0), respectively, for a particle in 0.15 mM KOH. The center of oscillations was calculated by averaging the minimum and maximum heights of the particle (during the last full cycle). The difference between this average and $h(0)$ was reported as the displacement in Fig. 8(c), which shows that the center of oscillations of a particle moved away from the electrode with increasing electric field strength. The linear model predicts no displacement in the center of oscillations. Figures 8(a) and 8(b) show that the nonlinear model produced phase angles and amplitudes nearly identical to those produced by the linear model over the entire range of electric field strengths.

V. DISCUSSION

A. Source of electrolyte dependence of the phase angle

The dependence of aggregation or separation of particles on electrolytes has been a paradox to the present investigators for many years [10,13,14,16–18,22–24]. The gross response of particles to imposed ac polarization depends weakly on the nature of the electrolyte. However, the result is a binary difference, aggregation or separation. Figure 6(c) resolves this core paradox by showing that the subtle changes of phase angle associated with differences among electrolytes are otherwise inconsequential except that one observes opposite behavior on one side of 90° or the other. Phase angles >90° cause particles to separate while phase angles <90° cause particles to aggregate. This sensitivity explains the discovery that a change of anion from Cl^- to OH^- changes the gross behavior of particles from aggregation to separation [18]; indeed, the 90° boundary is a razor's edge that sharply separates particle separation and attraction.

At 500 Hz, one set of electrolytes (KCl, $NaHCO_3$) had a phase angle >90° and another set (KOH, NH_4OH, and NaOH) had a phase angle of <90°. Based on Fagan's drift velocity model and the results calculated here, particles in KCl and $NaHCO_3$ are predicted to aggregate while those in KOH, NH_4OH, and NaOH are predicted to separate at 500 Hz. Each of these predictions matched experimental observations.

The primary origin of electrolyte dependence was the difference in the complex DEM of each electrolyte, specifically the phase angle. Figure 4 shows that the DEM phase angle was different for each electrolyte in the frequency range tested here. An external electric field breaks the particle's azimuthal charge symmetry (see Fig. 9); the concentration of cations at one pole of a negatively charged particle decreases and the concentration of anions at the opposite pole of the particle increases. Consequently, the particle and its diffuse cloud acquire a net dipole moment. This dipole moment disturbs the local electric field; a reverse component (sometimes called the "back" electric field, E_b) restores the equilibrium structure of the diffuse layer. Along the surface of the particle, E_b generally acts oppositely to the direction of the applied electric field.

The DEM phase angle is a consequence of the finite time required for the redistribution of ions in the diffuse layer in response to a change in the applied electric field. In contrast, the back electric field E_b responds instantaneously to the distribution of ions around the particle. The particle responds to the sum of the applied and back electric fields. As frequency

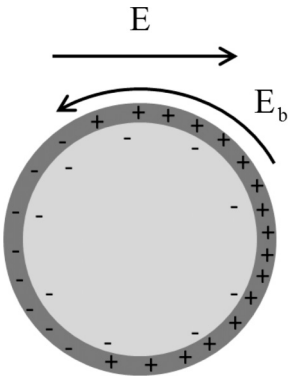

FIG. 9. Illustration of diffuse layer polarization. Both the external electric field E and back electric field E_b oscillate, but are not necessarily in phase. The phase difference between these two electric fields causes a phase angle in the dynamic electrophoretic mobility of the particle.

$\rightarrow$ 0 Hz, the phase angle between the external and back electric fields approaches 180°; i.e., the electric fields are in phase, but are opposite in sign. In this frequency regime, the sum electric field produces a DEM phase angle of 0° [see Fig. 4(b)] because the ions in the diffuse cloud can achieve their equilibrium distribution at each instant of time. As the frequency increases above 0 Hz, the redistribution of ions in the diffuse cloud (affecting the back electric field) does not respond instantaneously. The delayed response of the back electric field causes the sum electric field to lead the applied electric field, which drives the mobility phase angle to increase above 0°. As the frequency of the external electric field is further increased, the inertia of both the particle and displaced fluid increases in importance and the mobility phase angle drops below 0°. The balance between the dynamic transport of ions and the particle-fluid inertia causes a maximum in the mobility phase angle. Clearly, the ion's diffusion coefficient must affect this balance.

The effect of the anion's diffusion coefficient D_- on the DEM was calculated by systematically varying the value of the anion diffusion coefficient and fixing the cation's diffusion coefficient at 2.66×10^{-5} cm^2/s. Figure 10 shows the DEM phase angle for three values of D. The anion (co-ion to the charge of the particle) had a substantial impact on the DEM phase angle, which is important because a larger DEM phase angle corresponds to a particle phase angle farther from 90°. This behavior is illustrated in Fig. 4. For electrolytes with the same cation (KOH and KCl, NaOH and $NaHCO_3$), the DEM phase angle was larger for the electrolyte with an anion having a larger diffusion coefficient. The importance of the co-ion to the DEM phase angle might surprise some readers because the concentration of co-ions in the diffuse layer is much smaller than the concentration of counterions.

The secondary origin of the electrolyte dependence of the phase angle was the previously neglected difference in bulk electrolyte conductivity. Electrolyte solutions with a larger conductivity had a smaller electric field at fixed frequency below 50 Hz [see Fig. 6(a)]. An increase in electric field strength increased the value of the phase angle [see Fig. 8(a)], provided the electric field was $>\sim$250 V/m. Thus, electrolytes

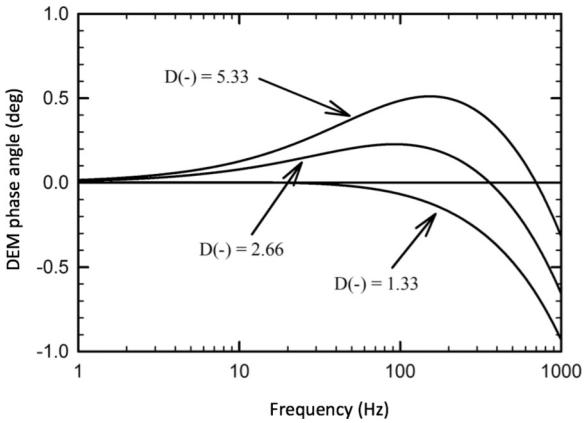

FIG. 10. The dynamic electrophoretic mobility (DEM) phase angle of a particle dispersed in electrolyte with systematically different anion diffusion coefficients. $D(-)$ is the value of the diffusion coefficient of the anion (co-ion to the charge of the particle) and has units of 10^{-5} cm^2/s. The value of the cation (counterion) diffusion coefficient was held fixed at 2.66×10^{-5} cm^2/s. These data illustrate the importance of the diffusion coefficient of the co-ion. A larger value of the co-ion diffusion coefficient produced a larger DEM phase angle and, thus, a lower particle position phase angle.

with a small conductivity (and larger electric field strength at fixed frequency) tended to have a larger phase angle at fixed ionic strength.

B. Comparing the linear and nonlinear models

Figures 7 and 8 show that the linear and nonlinear models produce very similar results. In particular, Figs. 8(a) and 8(b) show that the two models produce nearly identical phase angles and amplitudes for a wide range of electric field strengths. The main difference between the two models is the displacement in the center of oscillations: the linear model predicts no shift in the center regardless of electric field strength, but the nonlinear model predicts a significant shift in the center away from the wall [see Fig. 8(c)]. Indeed, when the amplitude of the oscillations in elevation exceeds $h(0)$, the presence of an impenetrable wall forces a shift outward. The impenetrability of the wall is manifested in the nonlinear model as an exponentially increasing double-layer repulsion as the particle approaches the wall. By contrast, the colloidal forces are modeled as a linear spring, which are symmetric about $h(0)$, in the linear model.

While the linearization of the colloidal forces can explain the differences in the displacement in the center of oscillations predicted by the two models, it does not affect the predictions of phase angles or of the amplitude of those oscillations because colloidal forces are not a significant factor in Eq. (1) after the initial transient has expired and stationary oscillations occur. Wirth *et al.* [24] used the linear model to investigate the relative importance of various forces appearing in Eq. (1) on the stationary oscillations in elevation as a function of frequency (see Fig. 11 in Ref. [24]). At 100 Hz (the frequency used in Figs. 7 and 8), the applied electrophoretic force was balanced (to about 90%) by the quasisteady Stokes drag term in Eq. (6). In the linear model of Ref. [24], the particle was far from any wall and $f_\infty = 6\pi\eta a$ was used as the drag coefficient. In the linear model considered here, we partially account for the effect of the nearby wall by using a drag coefficient of $f_\infty/q[h\,(0)]$. The inclusion of the wall correction q^{-1} increases the drag coefficient by an order of magnitude, which increases the range of frequencies for which the applied electrophoretic force is balanced by the quasisteady Stokes drag. In other words, at frequencies near 100 Hz, Eqs. (1), (9), and (10) can be approximated by neglecting inertia, colloidal forces, the Basset force, and the dielectrophoretic force, leaving only quasisteady Stokes drag and the electrophoretic force:

$$\frac{f_\infty}{q\,[h(0)]}\frac{dh}{dt} = QE\,(t) = \frac{f_\infty \mu}{q\,[h\,(0)]}E(t). \tag{24}$$

Since the same value of the drag coefficient is used in both of the remaining terms, it vanishes from the equation, leaving

$$\frac{dh}{dt} = \mu E(t). \tag{25}$$

Thus the amplitude of oscillations given by Fig. 8(b) is—to a good approximation—just the integral of the electrophoretic velocity of the particle in an unbounded fluid over half of the cycle during which the electric field is pointing in the $+h$ direction. The main difference between the linear and nonlinear models in this case is that the nonlinear model uses a drag coefficient of $f_\infty/q[h\,(t)]$, which varies with time, whereas the linear model uses $f_\infty/q[h\,(0)]$, which is constant. Although the time dependence in the drag coefficient is substantial at high electric fields (for which the amplitude of elevation oscillations is substantial), since the drag coefficient cancels out in Eq. (24), the different values used in the two models are not important, which explains the good agreement seen in Fig. 8(b).

Equation (24) leads to a phase angle of 90° between $h(t)$ and $E(t)$, which is very close to the 88.5° reported in Fig. 8(a) for low electric field amplitudes for both the linear and nonlinear models. About 1° of this difference (between 90° and 88.5°) can be attributed to the dynamic electrophoretic mobility [see the KOH curve at 100 Hz in Fig. 4(b)]. The remainder arises in either model from small contributions from other forces neglected in the derivation of Eq. (24).

C. Limitations of the present model: Electrode effects

We have assumed that electroosmosis resulting from interaction of the imposed electric field with the diffuse cloud of the electrode did not contribute to the motion of the particle. Other investigators have shown that electroosmotic flow might be generated along the electrode surface and would contribute to the force experienced by the particle normal to the electrode [14,35]. For example, Yariv [35] investigated the $O(E)$ force experienced by a particle because of electroosmotic flow driven by the action of the electric field on the diffuse charge clouds of the surface of both the particle and the electrode. ICEO, which scales with the square of the electric field ($\sim\tilde{E}^2$) [15], might contribute force in the normal direction. Even a small effect of ICEO on the phase angle could cause a difference between aggregation and separation of particles because the phase angle is close to 90°. Both of these effects (equilibrium and induced charge electroosmosis) probably contribute to electrolyte dependence in the value of

the phase angle, but we are unaware of any treatment of these effects where the diffusion coefficients of the ions in solution are unequal.

VI. CONCLUSIONS

An *a priori* prediction of electrolyte-dependent particle motion in the direction normal to an electrode undergoing ac polarization was presented. The solution to the nonlinear integro-differential equation of motion of a particle near an *ac* electrode was obtained with a successive approximation numerical algorithm. The algorithm was tested against a known solution of a linearized problem. Highly accurate results were obtained for the test problem. The full nonlinear integro-differential equation was solved for a particle in KOH, KCl, $NaHCO_3$, NH_4OH, or NaOH with a full description of the dynamic electrophoretic mobility (DEM) of the particle. The phase angle and amplitude of oscillation were found to be electrolyte dependent. The calculated phase angles for a particle in KOH, NH_4OH, and NaOH were smaller than the phase angles calculated for a particle in KCl and $NaHCO_3$, which is consistent with experimental results. All phase angles collapsed to the 90° line, which is the razor's edge boundary between particle repulsion and attraction. Thus, the small difference in phase angle between electrolytes (~1°) was sufficient to predict separation for particles in some electrolytes and aggregation in others. Further, the family of curves for the amplitude of oscillation as a function of frequency was collapsed to a master curve by scaling the amplitude by the electric field strength and the DEM. There were two origins of this electrolyte dependence, (1) the complex dynamic electrophoretic mobility was electrolyte dependent and (2) the strength of the electric field was electrolyte dependent at frequencies <50 Hz. Future work should determine the full effect of electroosmotic flow (either equilibrium or induced charge) along the electrode on force experienced by the particle.

ACKNOWLEDGMENTS

The National Science Foundation supported this research under Grant No. CBET 0730391. The PPG Foundation, through the Achievement Rewards for College Scientists (ARCS) program, provided support for C.L.W. The Carnegie Institute of Technology also provided support to C.L.W. through a Bertucci graduate fellowship.

[1] J. D. Joannopoulos, P. R. Villeneuve, and S. H. Fan, Nature (London) **386**, 143 (1997).
[2] H. Zhou, L. R. White, and R. D. Tilton, J. Colloid Interface Sci. **285**, 179 (2005).
[3] S. Lecuyer, W. D. Ristenpart, O. Vincent, and H. A. Stone, Appl. Phys. Lett. **92**, 104105 (2008).
[4] P. J. Sides, C. L. Wirth, and D. C. Prieve, Electrochem. Solid State Lett. **13**, F10 (2010).
[5] C. L. Wirth, P. J. Sides, and D. C. Prieve, J. Colloid Interface Sci. **357**, 1 (2011).
[6] P. Richetti, J. Prost, and P. Barois, J. Stat. Phys. **39**, 254 (1985).
[7] M. Bohmer, Langmuir **12**, 5747 (1996).
[8] Y. Solomentsev, M. Bohmer, and J. L. Anderson, Langmuir **13**, 6058 (1997).
[9] M. Trau, D. A. Saville, and I. A. Aksay, Langmuir **13**, 6375 (1997).
[10] J. A. Fagan, P. J. Sides, and P. C. Prieve, Langmuir **18**, 7810 (2002).
[11] T. Y. Gong, D. T. Wu, and D. W. M. Marr, Langmuir **18**, 10064 (2002).
[12] J. Kim, S. A. Guelcher, S. Garoff, and J. L. Anderson, Adv. Colloid Interface Sci. **96**, 131 (2002).
[13] J. A. Fagan, P. J. Sides, and D. C. Prieve, Langmuir **19**, 6627 (2003).
[14] J. A. Fagan, P. J. Sides, and D. C. Prieve, Langmuir **20**, 4823 (2004).
[15] W. D. Ristenpart, I. A. Aksay, and D. A. Saville, Phys. Rev. E **69**, 021405 (2004).
[16] J. A. Fagan, P. J. Sides, and D. C. Prieve, Langmuir **21**, 1784 (2005).
[17] J. A. Fagan, P. J. Sides, and D. C. Prieve, Langmuir **22**, 9846 (2006).
[18] J. D. Hoggard, P. J. Sides, and D. C. Prieve, Langmuir **23**, 6983 (2007).
[19] W. D. Ristenpart, I. A. Aksay, and D. A. Saville, J. Fluid Mech. **575**, 83 (2007).
[20] Y. Liu, X. Y. Liu, and J. Narayanan, J. Phys. Chem. C **111**, 995 (2007).
[21] Y. Liu, R. G. Xie, and X. Y. Liu, Appl. Phys. Lett. **91**, 063105 (2007).
[22] J. D. Hoggard, P. J. Sides, and D. C. Prieve, Langmuir **24**, 2977 (2008).
[23] D. C. Prieve, P. J. Sides, and C. L. Wirth, Curr. Opin. Colloid Interface Sci. **15**, 160 (2010).
[24] C. L. Wirth, R. M. Rock, P. J. Sides, and D. C. Prieve, Langmuir **27**, 9781 (2011).
[25] F. Ma, S. Wang, L. Smith, and N. Wu, Adv. Funct. Mater. **22**, 4334 (2012).
[26] H. Brenner, Chem. Eng. Sci. **16**, 242 (1961).
[27] S. Kim and S. J. Karrila, *Microhydrodynamics: Principles and Selected Applications* (Butterworth-Heinemann, Boston, 1991).
[28] S. Ahualli, A. Delgado, S. J. Miklavcic, and L. R. White, Langmuir **22**, 7041 (2006).
[29] S. Ahualli, A. Delgado, S. J. Miklavcic, and L. R. White, J. Colloid Interface Sci. **309**, 342 (2007).
[30] B. H. Bradshaw-Hajek, S. J. Miklavcic, and L. R. White, Langmuir **24**, 4512 (2008).
[31] B. H. Bradshaw-Hajek, S. J. Miklavcic, and L. R. White, Langmuir **25**, 1961 (2009).
[32] B. H. Bradshaw-Hajek, S. J. Miklavcic, and L. R. White, Langmuir **26**, 1656 (2010).
[33] P. W. Dietz, J. Appl. Phys. **48**, 1036 (1977).
[34] R. W. O'Brien and L. R. White, J. Chem. Soc., Faraday Trans. 2 **74**, 1607 (1978).
[35] E. Yariv, J. Fluid Mech. **645**, 187 (2010).